ARL-TR-8206 ● Nov 2017

US Army Research Laboratory

Size Determination of Y_2O_3 Crystallites in MgO Composite Using Mie Scattering

by Zackery Fleischman, Victoria Blair, Larry Merkle, and Nicholas Ku

NOTICES

Disclaimers

The findings in this report are not to be construed as an official Department of the Army position unless so designated by other authorized documents.

Citation of manufacturer's or trade names does not constitute an official endorsement or approval of the use thereof.

Destroy this report when it is no longer needed. Do not return it to the originator.

ARL-TR-8206 ● NOV 2017

US Army Research Laboratory

Size Determination of Y_2O_3 Crystallites in MgO Composite Using Mie Scattering

by Zackery Fleischman and Larry Merkle
Sensors and Electron Devices Directorate, ARL

Victoria Blair and Nicholas Ku
Weapons and Materials Research Directorate, ARL

REPORT DOCUMENTATION PAGE		Form Approved OMB No. 0704-0188

1. REPORT DATE *(DD-MM-YYYY)*	2. REPORT TYPE	3. DATES COVERED (From - To)
November 2017	Technical Report	1 Feb 2017 – 30 Sept 2017

4. TITLE AND SUBTITLE	5a. CONTRACT NUMBER
Size Determination of Y_2O_3 Crystallites in MgO Composite Using Mie Scattering	5b. GRANT NUMBER
	5c. PROGRAM ELEMENT NUMBER

6. AUTHOR(S)	5d. PROJECT NUMBER
Zackery Fleischman, Victoria Blair, Larry Merkle, and Nicholas Ku	5e. TASK NUMBER
	5f. WORK UNIT NUMBER

7. PERFORMING ORGANIZATION NAME(S) AND ADDRESS(ES)	8. PERFORMING ORGANIZATION REPORT NUMBER
US Army Research Laboratory Sensors and Electron Devices Directorate (ATTN: RDRL-SEE-L) 2800 Powder Mill Road Adelphi, MD 20783	ARL-TR-8206

9. SPONSORING/MONITORING AGENCY NAME(S) AND ADDRESS(ES)	10. SPONSOR/MONITOR'S ACRONYM(S)
	11. SPONSOR/MONITOR'S REPORT NUMBER(S)

12. DISTRIBUTION/AVAILABILITY STATEMENT

Approved for public release; distribution is unlimited.

13. SUPPLEMENTARY NOTES

14. ABSTRACT

A computer program was developed to calculate the Mie scattering from yttrium oxide (Y_2O_3) crystallites embedded in a magnesium oxide (MgO) polycrystalline matrix. The calculation takes into account the volume fraction of Y_2O_3 in MgO, the average particle size, and the path length through the material to generate an expected light transmission spectrum. These calculated curves were compared to experimental transmission data obtained from prepared Y_2O_3/MgO nanocomposite materials to determine the average Y_2O_3 particle size. The results were used to determine optimal growth parameters leading to minimized scattering in subsequent material part preparation.

15. SUBJECT TERMS

nanocomposites, ceramic, laser, rare earth, erbium, scattering

16. SECURITY CLASSIFICATION OF:			17. LIMITATION OF ABSTRACT	18. NUMBER OF PAGES	19a. NAME OF RESPONSIBLE PERSON
a. REPORT	b. ABSTRACT	c. THIS PAGE			Zackery Fleischman
Unclassified	Unclassified	Unclassified	UU	24	19b. TELEPHONE NUMBER (Include area code) (301) 394-1142

Contents

List of Figures

List of Tables

Acknowledgments

We gratefully acknowledge the financial support from the US Army Research Laboratory (ARL) Director's Research Initiative Program.

This research was supported in part by an appointment to the Postgraduate Research Participation Program and ARL, administered by the Oak Ridge Institute for Science and Education through an interagency agreement between the US Department of Energy and ARL.

INTENTIONALLY LEFT BLANK.

1. Introduction

Lasers emitting in the mid-IR spectral region (2–6 μm) are of interest for use in a wide array of applications including atmospheric sensing,[1] wind lidar,[2] medical procedures,[3] IR countermeasures, molecular spectroscopy, and the optical pumping of longer wavelength solid-state lasers. Chief among the difficulties in developing efficient high-power-output mid-IR lasers is dealing with luminescence quenching by multiphonon relaxation (MPR). In general, the small energy transitions needed to generate mid-IR photons suffer more from this quenching process because fewer phonons are needed to bridge the energy gap between upper and lower laser levels, leading to a higher probability of nonradiative transitions. Therefore, when choosing a material to be a mid-IR gain medium, making sure it has a low maximum phonon energy will be crucial for minimizing quenching due to MPR.

Another important consideration when developing mid-IR lasers is that, even in efficient gain media, a significant fraction of the pump power is converted into waste heat. The amount of waste heat generated is at least partially determined by the quantum defect (QD) of the laser system, which is a measure of the difference between the pump photon energy and the output photon energy of the system. Unfortunately, mid-IR lasers often have a high QD because the pump photon energy is usually much larger than the output photon energy, meaning that the waste heat generated when operating at high power is substantial. This can be detrimental to laser operation in a number of ways including thermal lensing, which leads to poor beam quality, and thermally induced stress, which can cause the gain medium to fracture. To mitigate these problems, choosing a gain medium with high thermal conductivity is beneficial for efficient heat removal and overall thermal management.

There is often a trade-off in how effective one material can be at both providing high thermal conductivity and also small maximum phonon energy. It is generally the case that materials composed of lighter constituent atoms have the best thermal conductivity due to stronger restoring forces between the atoms. Unfortunately, this usually means that the material has greater maximum phonon energies. Conversely, materials composed of heavy atoms tend toward weaker forces and lower maximum phonon energies, but they are plagued by significantly lower thermal conductivities. This ultimately means that the likelihood of finding a single material that simultaneously offers high thermal conductivity and low maximum phonon energy is remote.

The solution to this trade-off might be found in nanocomposite materials. Nanocomposites are essentially ceramic or polycrystalline materials, which are

typically produced by sintering powdered precursor materials. Historically, nanocomposites were unattractive alternatives to single crystals because they tended to exhibit strong scattering at grain boundaries. However, refinements made in ceramic processing over the years have led to significantly improved optical properties, sometimes even rivalling their single crystal counterparts.[4,5] Other attractive aspects to ceramics are that their fabrication requires processing temperatures much lower than the melting temperature of a single crystal,[6] and more varied sizes and shapes are possible than in standard crystal growth. Furthermore, improvements in sintering equipment and powder handling techniques have made transparent, dual-phase nanocomposites within reach.[7] Such a dual-phase nanocomposite composed of equal parts yttrium oxide (Y_2O_3) and magnesium oxide (MgO) was recently prepared to combine the beneficial qualities of both materials, producing IR-transmitting windows with increased durability and thermal shock resistance.[8]

A dual-phase nanocomposite was developed to eliminate the described trade-off, incorporating a majority phase (MgO) chosen to offer high thermal conductivity and a minority phase (Y_2O_3) chosen for its low maximum phonon energy. The Y_2O_3 minority phase acts as host for the laser activator ion, in this work chosen to be the rare-earth element trivalent ion erbium (Er^{3+}). Early results showed promising fluorescence, but decent transmissivity remained elusive[9] because the degree of scattering in the materials was too great due to the mismatch in indices of refraction of the 2 species. To reduce optical scattering to laser and optical standards, the grain size of the constituents, especially the Y_2O_3 minority component, must be substantially smaller than the wavelength of light. Through optimization of the processing conditions, the grains have been driven to a smaller average size, and recent samples have demonstrated translucency sufficient to conduct the first light transmission studies of these materials.

In the current work, light transmission data are compared to the theoretical curves generated by the Mie scattering model in an attempt to determine the average grain size of the Y_2O_3 minority component in the dual-phase nanocomposites.

2. Experiment Details

Detailed preparation of the samples was thoroughly discussed in Blair et al.[9] In summary, a co-precipitation method was used to synthesize amorphous precursor powders of both phases together in an aqueous environment. Chemical precursors containing Y, Mg, and Er cations were combined in stoichiometric amounts to yield the desired composition target. The samples measured in the work covered by this report had 2.5% by weight $Er_{0.04}Y_{1.96}O_3$ and the balance MgO. Fine regulation of

the pH of the solution was necessary to maximize nucleation and minimize crystallite growth. After filtration, the resulting powder was washed in isopropyl alcohol, dried in an oven at approximately 65 °C, gently crushed, and then calcined at high temperature. The material was then densified by hot pressing, a technique where the sample is heated to high temperature within a die and pressed to 17 MPa under vacuum for varied dwell times. All samples were hot pressed in graphite dies with boron nitride (BN) spacers and the die wall coated with BN spray to limit carbon contamination of the part. The final product is a cylindrical pellet of ceramic with a diameter of approximately 25 mm and a thickness of approximately 1 mm.

The specific details for the samples measured in this study are in Table 1. The variations in calcination temperature–time and sintering temperature–time were implemented to determine how these parameters affect grain size, and thus transmissivity. Conventional wisdom dictates that higher processing temperatures should lead to larger grain growth. Some conditions were held constant across all the samples in this study. For instance, all samples were composed of 2.5 wt% Y_2O_3, and that component was doped with 0.8 at.% erbium. (However, the erbium content is inconsequential for this particular work.) The density of all the produced parts were measured using the Archimedes principle, and the percent of theoretical density (TD) was calculated based on a TD of the mixture being 3.616 g/cm^3.

Table 1 Sample preparation parameters and thicknesses for the dual-phase nanocomposite samples studied

Sample #	Powder calcine temp/time	Hot-press temp/dwell time	Sample thickness (cm)	Sample density (g/cm^3)	Percent of TD
1	1000 °C/30 min	1200 °C/30 min	0.114	3.597	99.5%
2	700 °C/30 min	1200 °C/30 min	0.118	3.601	99.6%
3	700 °C/30 min	1200 °C/10 min	0.171	3.562	98.5%
4	1000 °C/30 min	1200 °C/10 min	0.117	3.613	99.9%

To prepare for scanning electron microscopy (SEM), the samples were cut along the diameter into approximately one-quarter pieces. The cross section was ground flat using diamond-impregnated film and then mounted onto a sample holder and ion milled in a Leica TIC 3X for 4 h. The sample was then placed into the SEM and imaged without further treatment and using backscatter detection mode.

Figure 1 shows SEM micrographs of Sample 4 and Sample 1. Both powders were calcined at the same temperature, the only difference being the time the hot press dwelled at 1200 °C: 10 min and 30 min, respectively. The main feature of these images is the overall size of the Y_2O_3 (lighter phase) grains. Even though the material was as dense as it was going to get (both samples had a density greater

than 99% of TD), the Y_2O_3 grains are noticeably larger in the sample with longer hot-press dwell time (Sample 1). The banding effect that is also observed is likely due to the shear effects of uniaxial hot pressing in the die; this is often observed in ceramic blends.

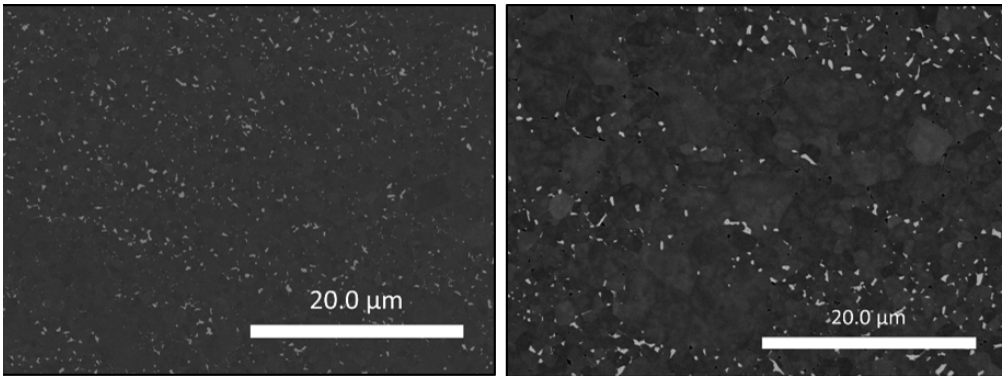

Fig. 1 SEM micrographs of Sample 4 (left) and Sample 1 (right)

To combat the inhomogeneity observed in Samples 1 and 4, a lower calcination temperature was used in the other samples. The idea was that this processing modification would serve to prevent agglomerates from forming during the calcination process. However, this synthesis technique requires a relatively high calcination temperature of 700 °C to remove all organic compounds. Indeed, Sample 2 (Fig. 2), which was calcined at 700 °C, does exhibit less of a banding effect and less segregation of the particles, likely due to a lower number of agglomerates.

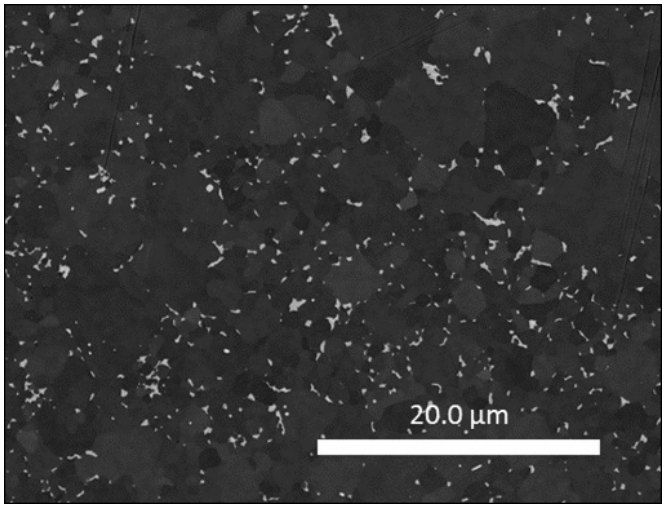

Fig. 2 SEM micrographs of Sample 2, calcined at 700 °C and hot pressed at 1200 °C for 30 min

Transmission (%T) measurements were performed on all samples using a Cary 6000i (UV-vis-nIR) spectrophotometer for measuring the 0.3- to 1.7-µm region and a Perkin Elmer Spectrum 2000 Fourier-transform infrared spectroscopy for measuring the 1.5- to 12-µm region. The results from both instruments were spliced together to complete the full transmission curve. Additionally, transmission measurements were performed on polycrystalline, undoped Y_2O_3 (Konoshima Chemical Co., Ltd, of Japan) and single-crystal undoped MgO (SPI Supplies, a division of Structure Probe, Inc., West Chester, Pennsylvania), the results of which are in Fig. 3. This information from the pure materials was necessary for the Mie scattering calculations described later.

Mie scattering calculations were carried out using a custom-made Labview program. The program takes the input parameters of scattering particle weight fraction f, the diameter of each scattering center a, the complex refractive indices of the host n_h and scattering particle n_p, and the overall thickness t of the composite sample to generate a percent transmission graph as a function of wavelength. All parameters except a are determined from direct measurements of the sample or, in the case of the complex refractive indices as a function of wavelength, were obtained from the respective Sellmeier equations and from the transmission measurements (Fig. 3). In practice, the desired experimental curve is loaded into the program along with the parameters relevant to that sample, and then a is incrementally adjusted until the best fit to the experimental data are achieved.

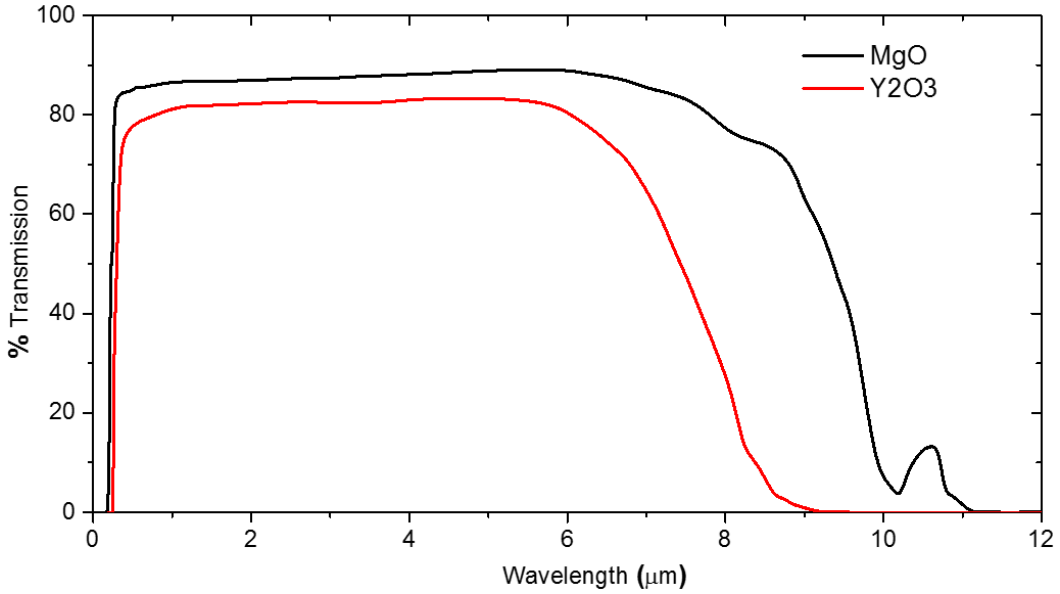

Fig. 3 Percent transmission of undoped ceramic Y_2O_3 and single-crystal MgO

3. Mie Scattering Theory

Mie scattering theory evolved as an extension of Rayleigh scattering.[10] While Rayleigh's theory is limited to describing the scattering of light from very small particles (diameter <1/10 wavelength), the Mie theory has no such limitation and can effectively handle scattering from particles larger than the wavelength of the incident light.[11] One of the hallmarks of Mie's theory is that larger particles scatter more strongly in the forward direction than in the backward direction, as shown in Fig. 4. Mie solutions converge to Rayleigh's as the particle size is decreased.

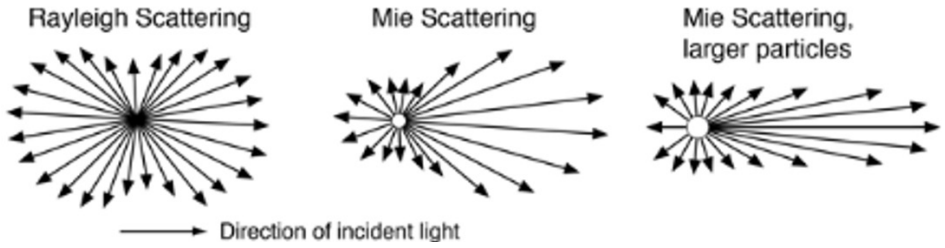

Fig. 4 Comparison of Rayleigh and Mie scattering profiles

Mie scattering theory seemed most appropriate in the endeavor of Y_2O_3 particle size analysis because, for this study's current batch of samples, the authors are confident that grains significantly smaller than the wavelength of light have not been achieved. The Mie scattering model employed considers a simplified system where the host material is nonabsorbing (true for MgO in the spectral region of interest) and the Y_2O_3 grains are considered to be spherical. Additionally, the model neglects the ceramic nature of the MgO host, assuming that scattering between MgO grains is negligible due to the matching index of refraction. Finally, the model does not account for the presence of additional impurities or porosity in the samples.

Since the authors wanted to compare the model's predictions to the experimental %T values, it seemed logical to start with Beer's Law:

$$T = (1 - R^2)\exp(-K_{ext}t), \tag{1}$$

wherein R is the Fresnel reflectance from the sample's surface, t is the sample thickness, and K_{ext} is the extinction coefficient, which includes loss contributions from absorption and scattering. Since the studied samples were composed mostly of MgO (97.5%), R was approximated using just that material's index of refraction. An expression for K_{ext} was derived in the dissertation of Eric Carl Fest for scattering of particles embedded in a composite medium.[12]

$$K_{ext} = 2\,\mathrm{Im}\left(\sqrt{k_h^2 + \frac{4if\pi S_{k_h}(0°)}{v_p k_h}}\right). \tag{2}$$

Here, f is the wt% of the scattering centers (in this case, the minority Y_2O_3 component) and v_p is the volume of a single scattering particle. The wavenumber in the host medium k_h is calculated using $k_h = 2\pi n_h/\lambda_0$ where n_h is the complex index of refraction of the host material and λ_0 is the wavelength in vacuum. The final undefined term in Eq. 2 is $S_{k_h}(0)$ which represents the Mie scattering matrix in the forward direction where $\theta = 0°$. This is sufficient for this study since the authors are comparing to measured transmission spectra, the only concern is about light travelling in the forward direction and not worrying about light scattered at a non-zero angle. Bohren and Huffman[13] provide an expression for the forward scattering matrix:

$$S_{k_h}(0°) = \frac{1}{2}\sum_{n=1}^{\infty}(2n+1)(a_n + b_n), \tag{3}$$

which was derived from the 2 × 2 scattering matrix relating incident and scattered electric fields. Here, a_n and b_n are the Mie scattering coefficients defined by

$$a_n = \frac{m\psi_n(mx)\psi_n'(x) - \psi_n(x)\psi_n'(mx)}{m\psi_n(mx)\xi_n'(x) - \xi_n(x)\psi_n'(mx)} \tag{4}$$

and

$$b_n = \frac{\psi_n(mx)\psi_n'(x) - m\psi_n(x)\psi_n'(mx)}{\psi_n(mx)\xi_n'(x) - m\xi_n(x)\psi_n'(mx)}, \tag{5}$$

which are described in terms of the Riccati-Bessel functions:

$$\psi_n(\rho) = \rho j_n(\rho) \tag{6}$$

and

$$\xi_n(\rho) = \rho h_n^{(1)}(\rho). \tag{7}$$

Equations 4 and 5 contain the size parameter x and the relative refractive index m defined by

$$x = \frac{2\pi\,\mathrm{Re}(n_h)a}{\lambda_0} \tag{8}$$

and

$$m = \frac{n_p}{n_h}, \tag{9}$$

where a is the scattering particle diameter, n_h and n_p are the complex indices of refraction of the host and scattering particle, respectively, and λ_0 is the vacuum wavelength of incident light.

The percent transmission can now be calculated for MgO/Y_2O_3 dual-phase composites using only a few parameters. Aside from the complex indices of refraction for the 2 materials (which do not vary from sample to sample), the authors just needed the Y_2O_3 particle diameter a, the Y_2O_3 volume fraction f, and the sample thickness t. Adjustment of any of these parameters will have an impact on the overall transmission curve, as shown in Fig. 5. The 3 curves in Fig. 5 each represent the changes to transmission as one of the parameters is doubled and then tripled, with the other 2 parameters held constant. Fig. 5a shows how variation of the a parameter leads to the greatest changes in the transmission curve at shorter wavelengths while having virtually no effect at the long wavelengths. Figure 5b exhibits a similar trend for variation of f; however, the changes are much less pronounced. Variation of t in Fig. 5c similarly has a weak effect on the shorter wavelengths; however, this is the only case where the longer wavelength portion of the spectrum is significantly altered. This is because the downward curve with increasing wavelength on the right side of the graph is related to increased material absorption, and absorption strength is strongly related to the path length through the sample (i.e., sample thickness).

Certain parameters are dictated by the specifics of each sample. For instance, all samples were prepared to have a Y_2O_3 volume fraction of 2.5%, and subsequent X-ray fluorescence analysis of the samples indicated that this was the case to within 10% error. According to Fig. 5b, a 10% variance in the f parameter should not significantly affect the fits. Additionally, the t parameter is even easier to determine simply by using a micrometer to measure the sample thickness. The t values for the 4 samples measured in this work were presented in Table 1. Thus, the a parameter should be the only one that needs to be adjusted when attempting to fit the experimental data.

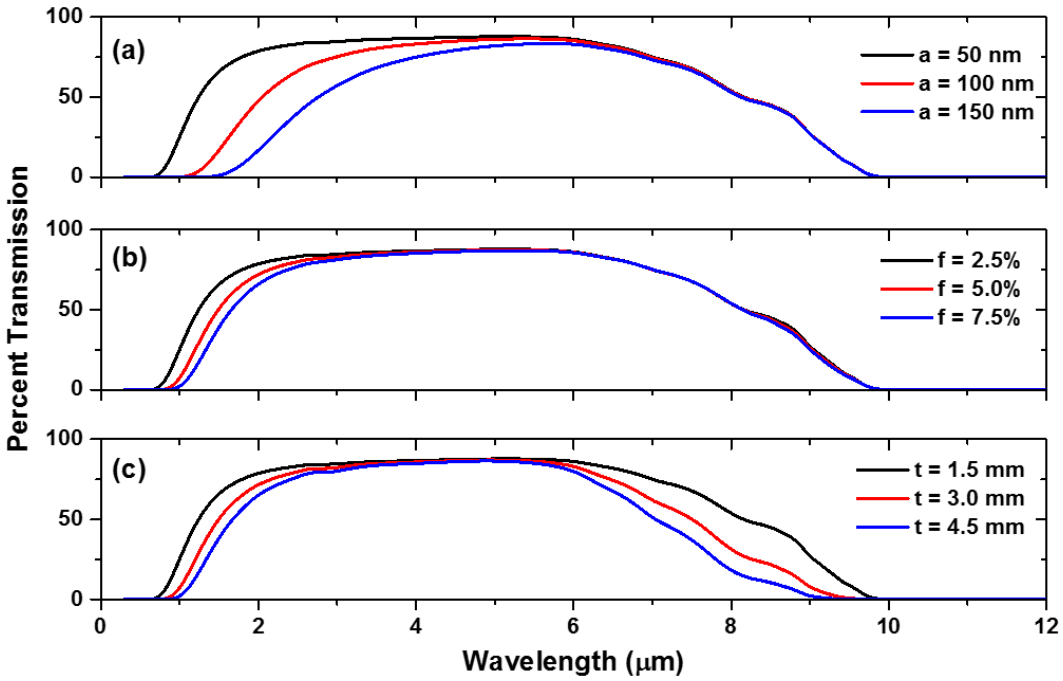

Fig. 5 Trends in the light transmission as one input is doubled and tripled while the other two are held constant: a) scattering particle diameter varied, b) Y_2O_3 volume fraction varied, and c) sample thickness varied

4. Results and Discussion

In the course of fitting the experimental transmission curves, the standard operating procedure was to attach priority to fitting the scattering band edge on the short-wavelength side of the curve and also try to conform to the high points of the curve as much as possible. The absorption edge on the long wavelength side of the graph was considered less important because it did not directly impact the *a* parameter determination. Unfortunately, in most cases, there could be found no *a* value that fit well in both high-priority regions. There seemed to be a trade-off between having a too-low fit on the left with a decent fit on the top, and having a decent fit on the left with a too-high fit on the top. In an effort to achieve fits in both regions, the authors tried a new tactic of implementing a <1 wavelength-independent scale factor *z* to the calculated fits. With adjustment of both *a* and *z*, decent fits were found for all samples. Such a broadband reduction in the calculated transmission curve is not unwarranted because the sample surfaces were not polished, which would lead to overall higher surface scattering losses. Figure 6 shows the recorded percent transmission spectra for the 4 MgO/Y_2O_3 nanocomposite samples measured in this study, as well as the *z*-modified fit curve for each. In addition, there is an "unmodified" fit that represents the same scattering calculation without employing the *z* factor.

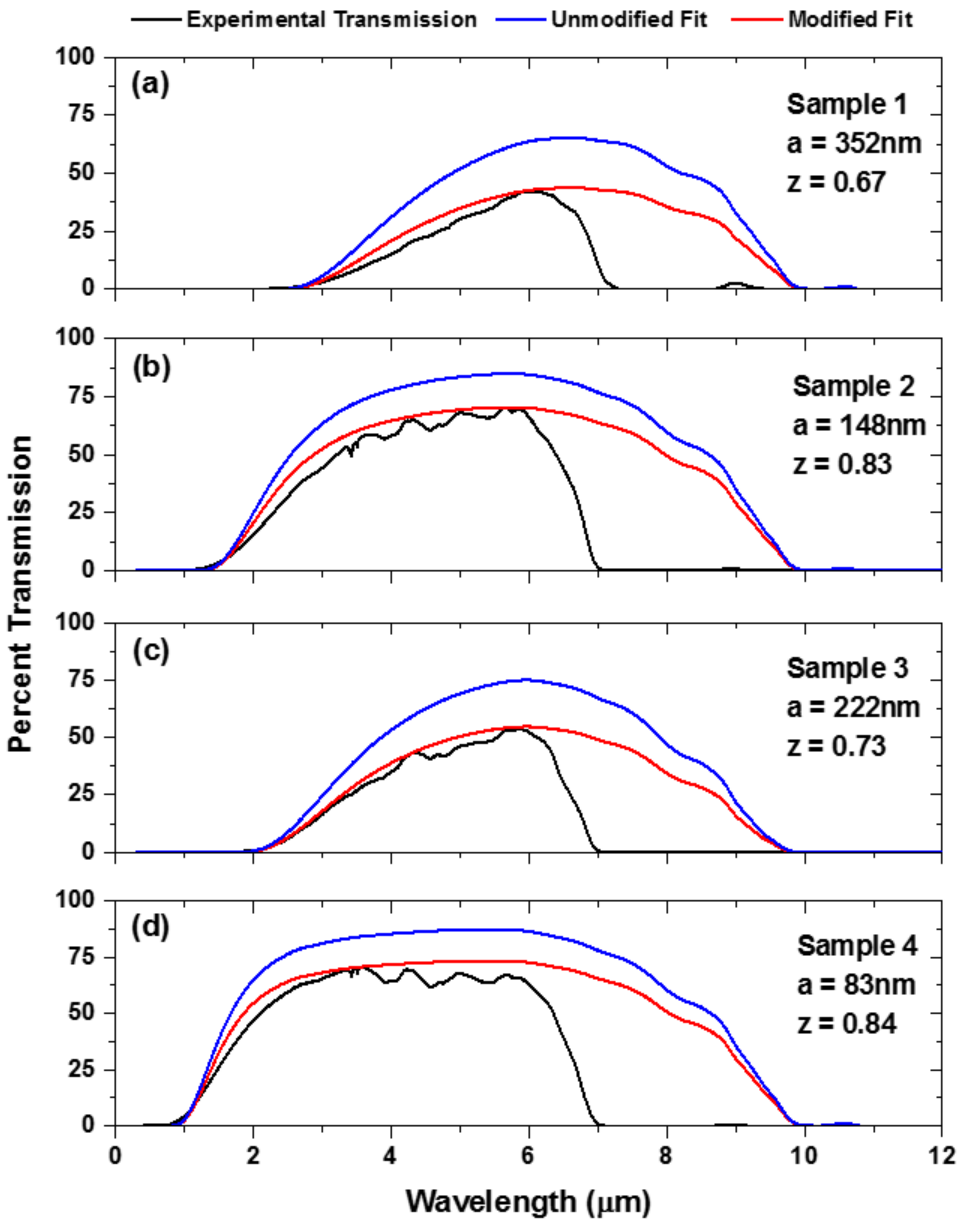

Fig. 6 Experimental percent transmission and 2 fit curves (best fit and maximum transmission possible) for the 4 MgO/Y_2O_3 nanocomposite samples measured; also scattering particle diameter *a* and modification factor *z* for each

The experimental curves in Fig. 6 show much more structure than is present in the fittings. The 2 main classes of structures observed are the relatively sharp absorption features toward the center of the graph and the rather sharp drop in transmission between 6 and 7 μm, which deviates significantly from theoretical predictions. The former is probably related to some amount of unknown impurities in the sample. The latter may well originate from unwanted BN contamination in the samples. Recall that BN was used to coat the die spacers during sintering.

Published infrared absorption spectra of BN show a strong absorption peak starting right around 6–7 microns.[14]

Figure 6 includes the *a* values used in calculating the curve fits for each sample. These range from 83 nm for Sample 4 to 352 nm for Sample 1. The clearest trend can be seen in these two bookend samples, both of which were calcined at 1000 °C for 30 min and both of which were hot pressed at 1200 °C. The difference between them, as shown in Table 1, is that Sample 1 was hot pressed for 30 min while Sample 4 dwelled at its max temperature for only 10 min. The extra time that Sample 1 was subjected to the high temperature treatment represents a much greater propensity for grain growth, and this was exhibited in the greater degree of scattering in this sample. These results correlate well with the relatively larger Y_2O_3 grain observed in the SEM image of Sample 1 shown in Fig. 1.

The fit curves for Samples 2 and 3 dictate *a* values in the middle of the range; however, these results did not follow as clear a trend. These samples contain material calcined at 700 °C for 30 min, with the same variation in hot-pressing times experienced by the previously discussed samples. One would expect that Sample 2, with its longer hot-pressing dwell time, would exhibit more scattering than Sample 3. Yet, the observations are just the opposite. Recall that the lower calcination temperature employed in the processing of these samples was chosen to reduce particle agglomeration. One possibility for this unexpected result is that the relatively low calcine temperatures resulted in material that was not fully nucleated, and that Sample 2, with its longer hot-press dwell time, was able to overcome this issue better than Sample 3 with its shorter hot-press dwell time. Such a phenomenon was observed in previous sample batches prepared at similar temperatures.

One final consideration that could explain the discrepancies between theoretical and experimental transmission is the porosity of the nanocomposites. The density of parts (listed in Table 1) is indicative of the remnant porosity in the samples. Any remnant porosity in these parts will influence the raw transmittance of the part as the pores will have a refractive index of the atmosphere inside the pore. Since these were processed under a vacuum (on the order of 10^{-5} torr), it is reasonable to assume that the trapped pores are under vacuum. However, there is still the possibility of pores affecting the overall scattering in the samples. Future improvements to Mie scattering calculations will attempt to account for the scattering caused by the porosity.

5. Conclusions

This work represented the authors' first attempt to use Mie scattering theory to determine Y_2O_3 grain size in prepared MgO/Y_2O_3 dual-phase nanocomposites. Theoretically, predicted transmission curves based on the adopted Mie scattering model were compared to experimentally obtained transmission data for samples processed at different temperatures. The observed transmission curves demonstrated various absorption phenomena, for which some of the sources the authors could reasonably identify (BN) and others remained uncategorized. Regardless of the type, these absorption features pointed toward a need for increased attention to reducing impurities during material preparation. Mixed results were observed when trying to correlate the authors' theoretically determined Y_2O_3 grain size to their expectations based on preparation temperatures. However, dispersion of the Y_2O_3 grain throughout the MgO matrix and overall grain size likely affected these results. Further processing modifications are actively being explored and revisions to the Mie scattering program to account for porosity are underway.

6. References

1. Taczak TM, Killinger DK. Development of a tunable, narrow-linewidth, cw 2.066-μm Ho:YLF laser for remote sensing of atmospheric CO_2 and H_2O. Appl Opt. 1998;37(36):8460–8476.

2. Hannon SM, Thomson JA. Aircraft wake vortex detection and measurement with pulsed solid-state coherent laser radar. J Mod Opt. 1994;41(11):2175–2196.

3. Kang HW, Lee H, Petersen J, Teichman JH, Welch AJ. Investigation of stone retropulsion as a function of Ho:YAG laser pulse duration. In: Kollias N, Zeng H, Choi B, et. al, editors. Proc. SPIE 6078, Photonic Therapeutics and Diagnostics II, 607815; 2006 Feb 22; San Jose (CA). Bellingham (WA): Society of Photo-Optical Instrumentation Engineers (SPIE); c2006. p. 188–198. doi:10.1117/12.646513.

4. Qi Y, Zhu X, Lou Q, Ji J, Dong J, Wei Y. Nd:YAG ceramic laser obtained high slope-efficiency of 62% in high power applications. Opt Express. 2005;13(22):8725–8729.

5. Dong J, Shirakawa A, Ueda K, Yagi H, Yanagitani T, Kaminskii, AA. Laser-diode pumped heavy-doped Yb.YAG ceramic lasers. Opt Lett. 2007;32(13):1890–1892.

6. Kong J, Tang DY, Chan CC, Lu J, Ueda K, Yagi H, Yanagitani T. High-efficiency 1040 and 1078 nm laser emission of a Yb:Y2O3 ceramic laser with 976 nm diode pumping. Opt Lett. 2007;32(3):247–249.

7. Xu S, Li J, Kou H, Shi Y, Pan Y, Guo J. Spark plasma sintering of Y2O3-MgO composite nanopowder synthesized by the esterification sol-gel route. Ceram Int. 2015;41(2):3312–3317.

8. Harris DC, Cambrea LR, Johnson LF, Seaver RT, Baronowski M, Gentilman R, Nordahl CS, Gattuso T, Silberstein S, Rogan P, et al. Properties of an infrared-transparent MgO:Y_2O_3 nanocomposite. J Am Ceram Soc. 2013;96 (12):3828–3835.

9. Blair VL, Fleischman ZD, Merkle LD, Ku N, Moorehead CA. Co-precipitation of rare-earth-doped Y_2O_3 and MgO nanocomposites for mid-infrared solid-state lasers. App Opt. 2017;56(3):B154–B158.

10. Rayleigh L. On the light from the sky, its polarization and color. Philos Mag. 1871;41;107–120.

11. Mie G. Beitrage zur optik trüber medien, speziell kolloidaler metallösungen. Ann Phys 25.1908:330(3);377–445.

12. Fest EC. Modelling scatter in composite media [dissertation]. [Tucson (AZ)]: University of Arizona; 2008.

13. Bohren CF, Huffman DR. Absorption and scattering of light by small particles. New York: Wiley; 1983.

14. Chore SM, Chaudhari GN, Manorama SV, Bath A. Structural and electrical properties of cubic boron nitride thin films on (100)GaAs. Semicond Sci Tech. 2002;17(11):1141–1143.

List of Symbols, Abbreviations, and Acronyms

%T	transmission
a	scattering particle diameter
ARL	US Army Research Laboratory
BN	boron nitride
Er	erbium
f	Y_2O_3 volume fraction
IR	infrared
K_{ext}	extinction coefficient
MgO	magnesium oxide
MPR	multiphonon relaxation
QD	quantum defect
SEM	scanning electron microscopy
t	sample thickness
TD	theoretical density
Y_2O_3	yttrium oxide; yttria

1 (PDF) DEFENSE TECHNICAL INFORMATION CTR DTIC OCA

2 (PDF) DIR ARL
IMAL HRA
RECORDS MGMT
RDRL DCL
TECH LIB

1 (PDF) GOVT PRINTG OFC
A MALHOTRA

15 (PDF) DIR ARL
RDRL SE
K KAPPRA
M WRABACK
RDRL SEE
G WOOD
RDRL SEE L
Z D FLEISCHMAN
L MERKLE
M DUBINSKIY
A MOTT
RDRL WM
J ZABINSKI
A RAWLETT
RDRL WMM
M VANLANDINGHAM
B DOWDING
RDRL WMM E
V L BLAIR
N KU
S SILTON
L VARGAS GONZALEZ